NANO LETTERS

2006
Vol. 6, No. 8
1812−1816

Raman Spectroscopy of Single-Wall Boron Nitride Nanotubes

R. Arenal,*,†,‡ A. C. Ferrari,§ S. Reich,§,|| L. Wirtz,⊥ J.-Y. Mevellec,# S. Lefrant,# A. Rubio,+,∞ and A. Loiseau†

Laboratoire d'Etude des Microstructures, ONERA-CNRS, 92322 Châtillon, France, Materials Science Division, Argonne National Laboratory, Argonne, Illinois 60439, Department of Engineering, University of Cambridge, Cambridge CB2 1PZ, U.K., Department of Materials Science and Engineering, Massachusetts Institute of Technology, Cambridge, Massachusetts 02139-4307, Institut d'Electronique, de Microélectronique et de Nanotechnologie (IEMN), BP 60069, 59652 Villeneuve d'Ascq Cedex, France, Laboratoire de Physique Cristalline, Institut des Matériaux Jean Rouxel, BP 32229, 44322 Nantes, France, and Institut fuer Theoretische Physik, Freie Universität Berlin, D-14195 Berlin, Germany, and European Theoretical Spectroscopy Facility (ETSF)

Received February 2, 2006; Revised Manuscript Received June 2, 2006

ABSTRACT

Single-wall boron nitride nanotubes samples synthesized by laser vaporization of a hexagonal BN target under a nitrogen atmosphere are studied by UV and visible Raman spectroscopy. We show that resonant conditions are necessary for investigating phonon modes of BNNTs. Raman excitation in the UV (229 nm) provides preresonant conditions, allowing the identification of the A_1 tangential mode at 1370 cm^{-1}. This is 5 cm^{-1} higher than the E_{2g} mode in bulk h-BN. Ab initio calculations show that the lower frequency of bulk h-BN with respect to large diameter nanotubes and the single sheet of h-BN is related to a softening of the sp^2 bonds in the bulk due to interlayer interaction.

Boron nitride nanotubes (BNNTs) have complementary properties to those of carbon nanotubes (CNTs). They can be considered as a single sheet of hexagonal BN (h-BN) rolled upon itself. BNNTs possess a band-gap larger than 5.5 eV—independent of their diameter and chirality.[1] This makes BNNTs promising materials for applications in nanoelectronics[2] and optoelectronics (blue-light emitters, excitonic lasers, etc.). The experimental study of their properties has been limited for a long time by the lack of samples in sufficient quantity, the first syntheses being restricted to very low yields. Thanks to a new synthesis technique based on the vaporization of a h-BN target by a continuous laser under a nitrogen atmosphere,[4] single-wall BNNTs (SW-BNNTs) can now be produced routinely in gram quantities. High-resolution transmission electron microscopy (HRTEM), electron energy loss spectroscopy (EELS),[3−5] transport experiments,[2] measurements of the optical properties by means of absorption,[6] and low-loss EELS[3,8] were performed on these tubes. These measurements confirmed the predicted large band gap.[1,3,8]

In a recent work, we studied the phonons of SW-BNNTs using density functional theory.[9] Raman intensity calculations[10,11] predicted the most intense peak in the spectra to be due to the transverse optical A_1 mode, which can be constructed via zone folding from the Raman active optical E_{2g} mode (1365 cm^{-1}) of h-BN.[12−14] Previous Raman experiments on BNNTs were done on double-wall and multiwall samples and yielded contradictory results,[15−17] as we discuss later. In this Letter, we measure the vibrational properties of SW-BNNTs using Raman spectroscopy in the UV and visible range.

The synthesis of the SW-BNNT used in this study is described elsewhere.[4,5] The collected synthesis products are studied by HRTEM, using Philips CM20 (200 kV) and JEOL 4000FX (400 kV) microscopes.[3,5] The raw powder is very inhomogeneous. Some areas consist of nanosized objects and are rich in NTs. Other regions are rich in large size h-BN platelets, which, in some cases, can be up to several

* Corresponding author. E-mail: arenal@anl.gov.
† Laboratoire d'Etude des Microstructures, ONERA-CNRS.
‡ Materials Science Division, Argonne National Laboratory.
§ Department of Engineering, University of Cambridge.
|| Department of Materials Science and Engineering, Massachusetts Institute of Technology.
⊥ Institut d'Electronique, de Microélectronique et de Nanotechnologie (IEMN).
Laboratoire de Physique Cristalline, Institut des Matériaux Jean Rouxel.
+ Institut fuer Theoretische Physik, Freie Universität Berlin, and European Theoretical Spectroscopy Facility (ETSF).
∞ Permanent address: Dpto. Física de Materiales, Facultad de Químicas, U. País Vasco, CSIC-UPV/EHU, and Donostia International Physics Center, 20018 San Sebastián, Spain.

10.1021/nl0602544 CCC: $33.50
Published on Web 07/06/2006

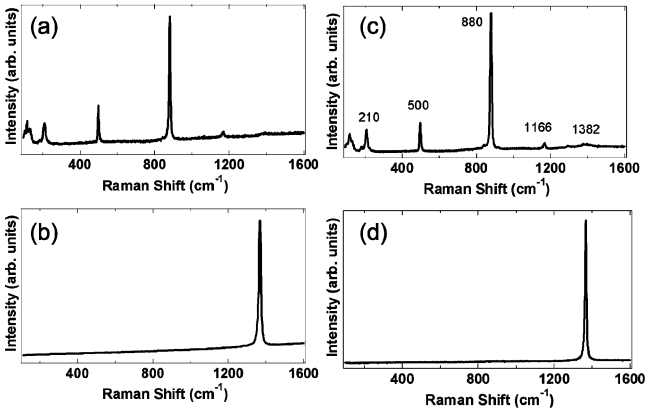

Figure 1. Raman spectra excited at 514.5 nm: left, (a) and (b) acquired on different areas of the raw synthesis products; right, spectra of highly pure commercial powders of (c) boric acid and (d) h-BN.

micrometers in size. These are fragments of the target expelled by the laser. We carefully verified the chemical composition of the NTs and nanoparticles by spatially resolved EELS.[3,5] BNNTs are in majority SW, either isolated or organized in small bundles (2−10 tubes), with some (∼20%) multiwall (primarily double wall) NTs. The tube diameters are close to 2 nm. The size of the nanoparticles is over 20 nm. These are composed of boron and sometimes covered by by a thin boron oxide (B_2O_3) layer and wrapped into a cage of several h-BN concentric layers.[3] Sometimes these cages are empty.

Raman spectra are measured at 229, 244, and 514 nm excitations using Renishaw micro-Raman 1000 spectrometers. The UV Raman spectra are collected with a 40× objective and a UV-enhanced charge-coupled device camera. The spectral resolution is ∼8 cm^{-1}. For visible excitation we use 50× and 100× objectives, and the spectral resolution is ∼2 cm^{-1}. All the UV Raman spectra are corrected by subtracting the background signal due to the optics. This is done by measuring an Al mirror background signal and normalizing all spectra to the atmospheric N_2 peak at ∼2332 cm^{-1}.

Due to the inhomogeneity of the raw synthesis samples, recording Raman spectra was a very delicate task. We used a laser spot size of 1 μm and took advantage of this inhomogeneity for exploring different areas in the soot. Depending on the position of the spot, we observe mainly two kinds of spectra, when exciting with 514 nm, parts a and b of Figure 1. These spectra can be understood by comparing them with spectra obtained on high-purity commercial reference samples (Goodfellow) shown in parts c, boric acid (H_3BO_3), and d, h-BN, of Figure 1. The spectrum in Figure 1a has a dominant peak at 880 cm^{-1} and some smaller peaks at 210, 500, and 1166 cm^{-1}. These peaks represent the typical spectrum of boric acid;[18] see Figure 1c. Boric acid is known to form very easily from the spontaneous reaction of boron and boron oxide (B_2O_3) with moisture and oxygen in air. We explain its formation in the reactor as follows.[5] Upon heating by the laser, h-BN crystallites of the target decompose above 2700 K into nitrogen gas and liquid boron which becomes finally gaseous. Boron oxide contained in the binder of the target also decomposes above 2133 K to give rise to gaseous boron. This boron gas phase is then quenched in the synthesis chamber and condenses into small liquid droplets that either react with nitrogen to produce nanotubes or BN cages[4,5] or simply solidify. In the latter case, the resulting boron particles transform progressively into boric acid by contact with air after opening the reaction chamber and collecting the soot. The presence of boric acid is also confirmed by infrared spectroscopy. The acid cannot be identified in transmission electron microscopy/electron energy loss spectroscopy (TEM-EELS) analysis because of the procedure used to prepare TEM grids. This involves dispersion of the soot in ethanol, which is known to dissolve boric acid.[19] We can estimate by differential scanning calorimetry measurements that the acid is about half of the soot.[5] This explains its easy detection in visible Raman measurements. The spectrum displayed in Figure 1b is very similar to that of Figure 1d indicating clearly that the response obtained on the soot corresponds to h-BN fragments expelled from the target during the ablation as already identified by TEM. The dominant feature of the spectra is a peak at 1366 cm^{-1} which corresponds to a E_{2g} mode of h-BN in agreement with previous works. No peak in the visible Raman spectra can be attributed to SW-BNNTs; all observed modes are due to contaminants or subproducts of the synthesis.

It is well-known that the phonon modes of C-NTs are observed under resonant conditions.[22,23] This is extensively used for probing the electronic structure of carbon tubes and determining their metallic/semiconducting character.[22,23] The electronic gap of BNNTs is estimated to exceed 5.5 eV from the calculations in refs 1, 20, and 21 and recent absorption and EELS experiments.[6,8] Then, to try and study phonon modes of SW-BNNTs by resonant Raman spectroscopy, we need to work in the UV range to get as close as possible to resonance. We thus performed UV−Raman measurements at excitation wavelength of up to 229 nm (5.41 eV). This is currently the shortest wavelength accessible in our micro Raman spectrometer. It must be noted, however, that 229 nm only allows preresonance conditions to be reached, as we will discuss later. The heterogeneity of the samples requires measurements on well controlled areas to be sure of measuring the SW-BNNTs and not some other h-BN particles. We first transfer each sample on a TEM grid and carefully map the sample morphology and composition in different regions on the grid. The micro-Raman spectra are then measured on specific areas characterized by TEM and marked on the grid prior to the Raman measurements. The use of the solvant (ethanol) in the TEM grid preparation is an additional advantage of this procedure, because it eliminates the boric acid from the sample. Figure 2 shows the TEM micrographs of two regions of the grid where the UV−Raman spectra were recorded. The area in Figure 2a has a high density of NTs, clearly visible in the high-resolution micrograph, Figure 2c. This area has more than 50% NTs, mixed with some small h-BN cages (their size is between 20 and 100 nm). Figure 2b corresponds to a platelet of h-BN of micrometer size, expelled from the target.

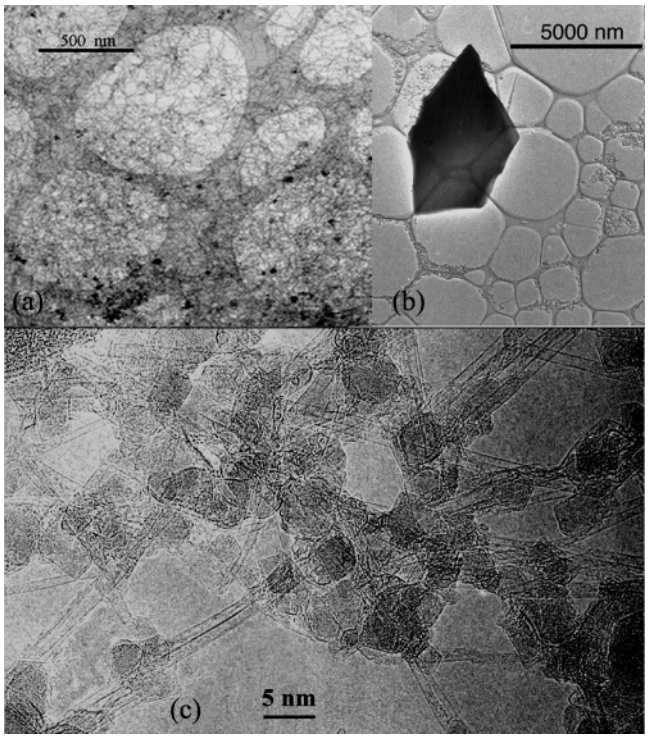

Figure 2. TEM images of the BN-NTs sample showing (a) a dense NTs area, (b) h-BN particle, and (c) HRTEM image of the NTs.

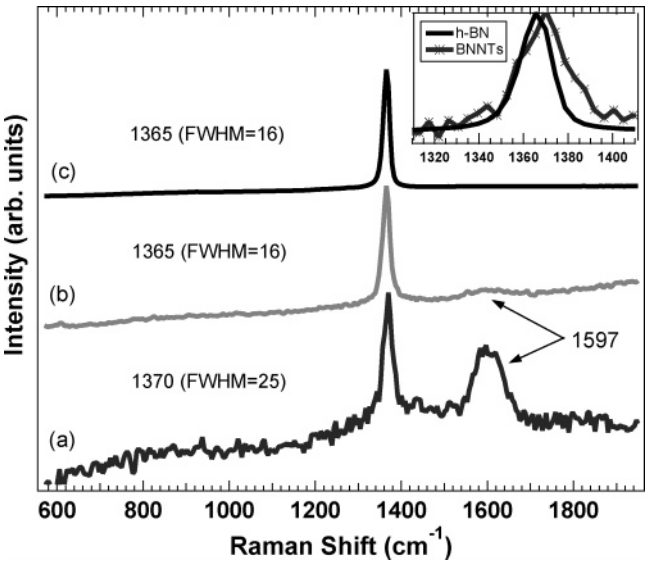

Figure 3. Raman spectra excited at 229 nm on (a) a BNNT-rich area in a standard TEM carbon grid (see Figure 2a,c), (b) a particle of h-BN on the same grid (Figure 2b), and (c) highly crystalline powder h-BN.

UV Raman spectra measured on the two areas, parts a and b of Figure 2, at the same power, are shown in spectra a and b of Figure 3, respectively. Figure 3c corresponds to the spectrum of a h-BN reference sample. The peak at 1597 cm^{-1} in spectra a and b of Figure 3, is due to the holey carbon membrane of the TEM grid. Our UV micro-Raman spectrometer has notch filters with a cutoff frequency of ~500 cm^{-1}. This is a general problem with all currently available single grating spectrometers and UV excitation.[15] Therefore, the BNNTs radial breathing modes (RBMs) at low frequencies cannot be detected in UV Raman measurements. These modes would be a unique and reliable signature of SW-BNNTs. The accessible modes are tangential modes at high frequencies. For h-BN, this mode is the E_{2g} mode at 1365 cm^{-1},[12−14] which is the main peak in spectra b and c of Figure 3. The spectrum recorded on the NTs area (Figure 3a) also has a peak in this frequency range, but this spectrum differs from h-BN (spectra b and c of Figure 3) in two ways as emphasized in the inset of Figure 3. The peak in the NT's spectrum is shifted to higher frequencies by 5 cm^{-1} and it is broadened asymmetrically. Although the shift in frequency observed is slightly below the resolution of the spectrometer, it was observed with the same magnitude on different spots of the sample. It is intrinsic of the NTs-containing areas.

An upshift and broadening of the E_{2g} mode are typical for small h-BN crystallites.[13] Nemanich et al.[13] established relationships between the h-BN frequency shift, the broadening of the mode, and the particle size. Using their formulas and taking into account the uncertainty from the spectral resolution, we find a crystallite size of ~10 nm. This appears to be inconsistent with our TEM observations of the h-BN cages present within the BNNT soot, having dimensions between 20 and 100 nm.[3,5] Using the dimensions from TEM, Nemanich's expressions predict an upshift of the E_{2g} mode of less than 1 cm^{-1}, much less than that found in Figure 3a. Moreover, the areas of our sample that were rich in BNNTs had a very low density of BN nanoparticles; see Figure 2a. Furthermore, if the shift and broadening in our UV experiment were due to h-BN cages, it must be observed in the visible Raman spectra as well. This is not the case as can be seen in Figure 1b. We never observed an upshift or broadening in the visible Raman spectra, even on the same TEM grid as used in the UV experiments. We therefore conclude that the spectrum in Figure 3a is not coming from h-BN cages.

We now consider whether the shift and broadening of the Raman peak in Figure 3a compared to that in Figure 3c can be due to laser heating or stress in the nanostructures. An increase in temperature or pressure both yield an increase in the anharmonicity of the E_{2g} phonon (line broadening). We did not apply any pressure to our samples, so this explanation seems unlikely; also, a stress or pressure-related effect should be observed in the visible spectra as well. The local temperature, on the other hand, can be different for visible and UV excitation because of the larger absorption coefficient in the UV and laser heating can be more pronounced in nanostructures than the corresponding bulk material.[24] However, an increasing temperature softens the E_{2g} phonons,[25] whereas we observe a hardening of the Raman line in the nanotube-rich areas, Figure 3a. We therefore conclude that the upshift of the main Raman line to 1370 cm^{-1} in Figure 3a is intrinsic for SW-BNNTs.

We thus assign the peak observed in the spectrum of Figure 3a to phonon modes of NTs and consider it as a composite signal due to the tangential A_g and longitudinal E_{2g} modes (assignment for armchair tubes, in the case of zigzag and chiral tubes the corresponding assignment is A_1 and E_g).[10] Calculated Raman spectra[10] predict two modes close

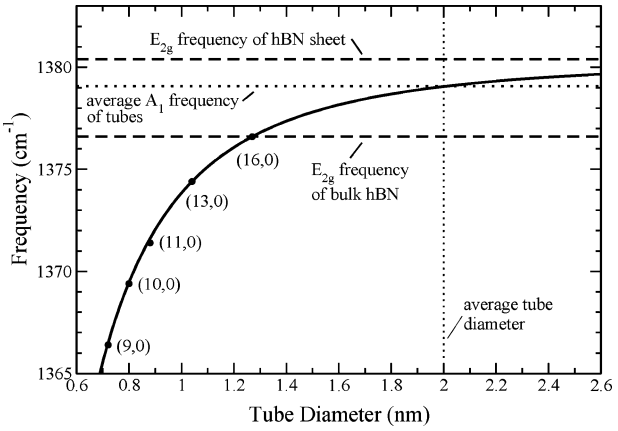

Figure 4. Calculated frequencies of the Raman active optical A_1 mode for different (n,0) zigzag BNNTs (symbols). The solid line is a fit (see text) that describes the convergence of the mode frequency with increasing tube diameter toward the value for the isolated sheet.

in frequencies. The E_{2g} mode is red-shifted with respect to the A_g mode and is less intense. This fits well with our experimental observations, where the broadening of the 1370 cm^{-1} peak could be due to a shoulder located on its left (low frequency) side. A recent calculation of the h-BN Raman susceptibility (square root of the Raman cross section) using its dielectric function[14] showed that the susceptibility increased by a factor of 5 between 514.5 and 229 nm. Resonance is, however, only achieved for a wavelength below 210 nm or an energy close to 6 eV, corresponding to the optical gap. Since for SW-BNNTs calculations and experiments indicate a gap close to that of h-BN, the result on the h-BN Raman susceptibility can be applied to the NTs. At 229 nm only preresonant conditions are achieved; i.e., we get a signal but it is weak. Our Raman experiments confirm an electronic gap of SW-BNNTs above 5.5 eV.

To understand the upshift of the 1370 cm^{-1} peak in the tube Raman spectrum (Figure 3a) with respect to the 1365 cm^{-1} peak in h-BN (Figure 3b,c), we compare with ab initio calculations of the phonon frequencies of nanotubes and bulk h-BN.[27] We showed[9] that the high-frequency A_1 mode of the tubes converges toward the E_{2g} frequency of a single sheet of h-BN. This is demonstrated in Figure 4 for zigzag nanotubes. Our calculations yield a frequency $\omega_{sheet} = 1380.4$ cm^{-1} for the single sheet. A fit of the calculated tube frequencies as a function of the diameter d yields $\omega(d) = \omega_{sheet} - 1268.3/d^{2.29}$ cm^{-1} (with d given in angstroms).[29] This functional form is also displayed in Figure 4. For the tubes with average diameter of 2 nm, the A_1 mode frequency is 1379.1 cm^{-1}, just 1.3 cm^{-1} below the E_{2g} frequency of the sheet.

Understanding the difference between the tube and bulk h-BN spectra thus essentially requires understanding the difference between the phonon frequency of the E_{2g} mode in bulk h-BN and the E_{2g} mode in the sheet. We calculated a frequency of 1376.6 cm^{-1} for the bulk, 3.8 cm^{-1} lower than for the sheet. This lower frequency is related to an increase of the calculated in-plane lattice constant, which is 4.718 a.u. for bulk h-BN and 4.714 a.u. for the single sheet. The difference stems from the—small but nonnegligible—interaction of neighboring sheets in bulk h-BN. The interaction leads to a small elongation of the B−N bond length and consequently a softening of the phonons. We note that while the calculations overestimate the absolute values of the frequencies (due to LDA, which is known to slightly underestimate the bond-length of most materials), they explain the frequency *difference* between bulk h-BN and the single sheet.[30] As demonstrated in Figure 4, the frequency shift of the tube phonon with respect to the phonon of bulk h-BN depends on the average tube diameter of the sample. In the present case, where the average diameter was measured to be about 2 nm, we calculated a blue shift of 2.5 cm^{-1}. Proper inclusion of van der Waals interaction in the bulk phase is expected to increase further this difference.[30]

Our results clarify the controversial works on multiwall BNNTs. Reference 15 reported a blue shift of the high-frequency BNNT peak ~2.1 cm^{-1} compared to bulk h-BN in UV Raman scattering. In contrast, ref 16 found a red shift of 3 cm^{-1} and ref 17 red shifts of 6 and 13 cm^{-1} for two different MW-BNNTs samples using visible excitation. Reference 15 detected a Raman peak at 920 cm^{-1} and assigned it to "disorder-induced Raman activity or contamination", since the authors considered it impossible for a perfect h-BN crystal to show such a feature. Reference 16 also stated that such a peak cannot be present in perfect h-BN crystals and considered this peak to correspond to the D peak in CNTs and graphite.[31] However, these assignments are incorrect, since the 920 cm^{-1} peak is observed in single-crystal h-BN and is just a second-order mode.[14] Zhi et al.[16] considered that the downshift and broadening of the high-energy mode at 1363 cm^{-1} in their spectra is due to the better crystallinity of their samples/NTs. However, since their tubes are large-diameter multiwall tubes, the Raman spectra should be similar to h-BN. We suggest that the downshift and broadening observed by Zhi et al.[16] are due to anharmonic effects (local temperature increasing by the laser) and unrelated to the NTs response, similarly for ref 17. The spectra in ref 15 show a smaller blue-shift than that found by us because their tubes contain two to eight layers. Then, the interaction between the nanotube walls accounts for the weaker hardening of this high-energy mode. Reference 15 reported also a peak at 880 cm^{-1} of unidentified origin that we assign to boric acid present in their samples.

In summary, SW-BNNTs samples have been studied by Raman spectroscopy using visible and UV excitation energies. Raman scattering in the visible range revealed a large fraction of boric acid, which was not detectable by TEM.[5,7] Identifying this contaminant is important, since it can hide the spectroscopic response of BNNTs. Raman scattering in the UV at 229 nm excitation provides preresonant conditions and allowed us to identify the tangential modes at high frequency (1370 cm^{-1}). The high-energy modes of SW-BNNTs are blue-shifted compared to the h-BN E_{2g} at 1365 cm^{-1}, because of the interaction of the neighboring sheets in h-BN. Our Raman experiments confirm also that the electronic gap of SW-BNNTs is larger than 5.5 eV.

Acknowledgment. This work was supported by the European Community networks COMELCAN (HPRN-CT-

2000-00128) and NANOQUANTA (NMP4-CT-2004-500198), by the French Grant "NABOCO", and by the GDR-E NanoE (No. 2756). We acknowledge helpful discussions with F. Ducastelle and J. P. Buisson. The authors are also grateful to A. Smith and I. R. Mendieta of University of Leeds and D. Wolverson of the University of Bath for the access to Raman facilities and their kind hospitality in their laboratories. We aknowledge G. Montagnac of the Ecole Normale de Lyon for the preliminary tests in Raman scattering in the UV. A.R. acknowledges the Humboldt Foundation under the 2005 Bessel research award. A.C.F. acknowledges funding from The Royal Society. Calculations were performed at the IDRIS supercomputing Center (Project 051827). We also thank the Barcelona Supercomputing Center, for computer resources and support.

References

(1) Rubio, A.; Corkill, J. L.; Cohen, M. L. *Phys. Rev. B* **1994**, *49*, 5081. Blase, X.; Rubio, A.; Louie, S. G.; Cohen, M. L. *Europhys. Lett* **1994**, *28*, 335.
(2) Radosavljevic, M.; Appenzeller, J.; Derycke, V.; Martel, R.; Avouris, P.; Loiseau, A.; Cochon, J.-L.; Pigache, D. *Appl. Phys. Lett.* **2003**, *82*, 4131.
(3) Arenal, R.; Stephan, O.; Kociak, M.; Taverna, D.; Colliex, C.; Rubio, A.; Loiseau, A. *AIP Conf.* **2004**, *723*, 293.
(4) Lee, R. S.; Gavillet, J.; Lamy de la Chapelle, M.; Loiseau, A.; Cochon, J.-L.; Pigache, D.; Thibault, J.; Willaime, F. *Phys. Rev. B* **2001**, *64*, 121405(R).
(5) Arenal, R. Ph.D. Thesis Université Paris XI, Orsay, 2005.
(6) Lauret, J. S.; Arenal, R.; Ducastelle, F.; Loiseau, A.; Cau, M.; Attal-Tretout, B.; Rosencher, E.; Goux-Capes, L. *Phys. Rev. Lett.* **2005**, *94*, 037405.
(7) Arenal, R.; Wirtz, L.; Mevellec, J.-Y.; Lefrant, S.; Rubio, A.; Loiseau, A. *AIP Conf.* **2003**, *685*, 384.
(8) Arenal, R.; Stephan, O.; Kociak, M.; Taverna, D.; Loiseau, A.; Colliex, C. *Phys. Rev. Lett.* **2005**, *95*, 127601.
(9) Wirtz, L.; Rubio, A.; Arenal, R.; Loiseau, A. *Phys. Rev. B* **2003**, *68*, 045425.
(10) Wirtz, L.; Lazzeri, M.; Mauri, F.; Rubio, A. *Phys. Rev. B* **2005**, *71*, 241402.
(11) Popov, V. N. *Phys. Rev. B* **2003**, *67*, 085408.
(12) Geick, R.; Perry, C. H.; Rupprecht, G. *Phys. Rev.* **1966**, *146*, 543.
(13) Nemanich, R. J.; Solin, S. A.; Martin, R. M. *Phys. Rev. B* **1981**, *23*, 6348.
(14) Reich, S.; Ferrari, A. C.; Arenal, R.; Loiseau, A.; Bello, I.; Robertson, J. *Phys. Rev. B* **2005**, *71*, 205201.
(15) Wu, J.; Wei-Qiang Han, Walukiewicz, W.; Ager, J. W., III; Shan, W.; Haller, E. E.; Zettl, A. *Nano Lett.* **2004**, *4* (4), 647.
(16) Zhi, C.; Bando, Y.; Tang, C.; Golberg, D.; Xie, R.; Sekigushi, T. *Appl. Phys. Lett.* **2005**, *86*, 213110.
(17) Yong Baea, S.; Seoa, H. W.; Park, J.; Choib, Y. S.; Parkc, J. C.; Leed, S. Y. *Chem. Phys. Lett.* **2003**, *374*, 534.
(18) Erdemir, A.; Bindal, C.; Zuiker, C.; Savrun, E. *Surf. Coat. Technol.* **1996**, *86*, 507.
(19) Lide, D. R. *Handbook of Chemistry and Physics*; CRC Press: New York, 2004.
(20) Marinopoulos, A. G.; Wirtz, L.; Marini, A.; Olevano, V.; Rubio, A.; Reining, L. *Appl. Phys. A* **2004**, *78*, 1157.
(21) Ng, M.-F.; Zhang, R. Q. *Phys. Rev. B* **2004**, *69*, 115417.
(22) *Carbon nanotubes*: *synthesis, structure, properties, and applications*; Dresselhaus, M. S., Dresselhaus, G., Avouris, Ph., Eds.; Springer-Verlag: Berlin, 2001.
(23) Reich, S.; Thomsen, C.; Maultzsch, J. *Carbon nanotubes*: *Basic concepts and physical properties*; Wiley-VCH: Berlin, 2004.
(24) Piscanec, S.; Cantoro, M.; Ferrari, A. C.; Zapien, J. A.; Lifshitz, Y.; Lee, S. T.; Hofmann, S.; Robertson, J. *Phys. Rev. B* **2003**, *68*, 241312.
(25) Exarhos, G. J.; Schaaf, J. W. J. *Appl. Phys.* **1991**, *69*, 2543.
(26) Kuzuba, T.; Sato, Y.; Yamaoka, S.; Era, K. *Phys. Rev. B* **1978**, *18*, 4440.
(27) Details of the calculations were presented in ref 9. Briefly, we use density-functional perturbation theory (DFPT) in the local-density approximation (LDA) as implemented in the code ABINIT.[28] Core electrons are replaced by Troullier-Martins pseudopotentials, and the valence electron wave functions are expanded in plane waves with an energy cutoff at 40 hartrees.
(28) Gonze, X.; et al. *Comput. Mater. Sci.* **2002**, *25*, 478.
(29) A similar scaling was also found in ref 11.
(30) The difference between the frequencies of sheet and bulk may even be larger than that calculated in this paper: the intersheet interaction in layered sp^2 bonded materials is usually underestimated by density-functional theory. The interaction contains two components: the first stems from the weak overlap of orbitals of neighboring sheets and is well described within DFT. The second contribution is due to van der Waals interaction and is completely neglected in the LDA (and equally poorly described by most other common exchange-correlation functionals). Proper inclusion of van der Waals effects would probably increase further the difference between sheet and bulk frequencies.
(31) Thomsen, C.; Reich, S. *Phys. Rev. Lett.* **2000**, *85*, 5214.

NL0602544